Effect of dynamical friction on nonlinear energetic particle modes

M. K. Lilley,[1,a)] B. N. Breizman,[2] and S. E. Sharapov[3]
[1]*Department of Earth and Space Sciences, Chalmers University of Technology, 41296 Göteborg, Sweden*
[2]*Institute for Fusion Studies, The University of Texas at Austin, Austin, Texas 78712, USA*
[3]*EURATOM/CCFE Fusion Association, Culham Science Centre, Abingdon OX14 3DB, United Kingdom*

(Received 13 July 2010; accepted 13 August 2010; published online 28 September 2010)

A fully nonlinear model is developed for the bump-on-tail instability including the effects of dynamical friction (drag) and velocity space diffusion on the energetic particles driving the wave. The results show that drag provides a destabilizing effect on the nonlinear evolution of waves. Specifically, in the early nonlinear phase of the instability, the drag facilitates the explosive scenario of the wave evolution, leading to the creation of phase space holes and clumps that move away from the original eigenfrequency. Later in time, the electric field associated with a hole is found to be enhanced by the drag, whereas for a clump it is reduced. This leads to an asymmetry of the frequency evolution between holes and clumps. The combined effect of drag and diffusion produces a diverse range of nonlinear behaviors including hooked frequency chirping, undulating, and steady state regimes. An analytical model is presented, which explains the aforementioned diversity. A continuous production of hole-clump pairs in the absence of collisions is also observed.
 [doi:10.1063/1.3486535]

I. INTRODUCTION

Energetic particles often excite Alfvén waves in toroidal magnetic confinement devices and similar instabilities may be driven by alpha particles and high-energy beam ions in ITER.[1] Observations of these waves provide important information about the plasma.[2] However, Alfvén waves can potentially enhance energetic particle losses from the plasma, which is undesirable.[1] It is therefore important, for burning plasmas, to predict and control the consequences of the wave-particle interaction. The nonlinear behavior of individual waves is an essential element of such research.

The present day experiments on Alfvén eigenmodes (AEs) reveal a rich family of nonlinear scenarios with several types of evolution of the wave amplitudes and frequencies. AEs excited by ion cyclotron resonance heating (ICRH)-produced ions show usually the "soft" excitation regimes.[3–8] In these nonlinear scenarios, the mode frequency remains close to the linear AE eigenfrequency and the structure of the mode remains similar to the linear one. In contrast, in the case of neutral beam injection (NBI), a "hard" nonlinear regime is observed more often, resulting in bursting amplitude evolution and in rapid frequency sweeping.[9–13] Spontaneous formation of phase space holes and clumps[14] is typical of the NBI-driven scenarios.[9] The holes and clumps in the energetic particle distribution function correspond to resonant particles that are trapped in the field of the wave. These nonlinear structures can be viewed as long living Bernstein–Greene–Kruskal (BGK) modes.[15]

The disparity between experiments on AE excitation by ICRH and NBI has recently been attributed to the role of dynamical friction (drag) as a relaxation process for resonant particles.[16] This observation was made in the bump-on-tail model for a near threshold instability with $|\gamma_L - \gamma_d| \ll \gamma_d \leq \gamma_L$, where γ_L is the energetic particle contribution to the wave growth rate and γ_d is the wave damping rate due to dissipation in the bulk plasma. In the past, such a model was successfully used to explain nonlinear bifurcations and frequency sweeping events observed in various AE experiments.[3,4,9]

It was found[16] that the mode grows explosively when dynamical friction (drag) dominates over velocity space diffusion in the vicinity of the wave-particle resonance. This previous analysis was limited to a weakly nonlinear regime with a perturbative treatment of the energetic particle response to the wave field. The present paper extends the analysis of Ref. 16 to describe the full nonlinear behavior in drag dominated scenarios. This is largely based on numerical modeling, which generalizes an earlier code[17] to include the effect of drag. We observe that the drag continues to play a destabilizing role in the fully nonlinear problem. It causes an asymmetric frequency sweeping pattern by enhancing the holes and suppressing the clumps. In addition, the combined effect of drag and velocity space diffusion creates an interesting range of nonlinear behaviors including hooked frequency chirping, undulating, and steady state regimes.

The remainder of this paper is organized as follows: Sec. II describes the basic equations of the bump-on-tail model, Sec. III deals with benchmarking of the numerical code (named BOT) against analytical theory, Sec. IV presents the formation and evolution of holes and clumps in the collisionless, drag dominated, and drag+diffusion cases, Sec. V summarizes the results, and the Appendix describes the numerical algorithm.

II. THE MODEL

Despite the specifics of the idealized bump-on-tail model,[18] the nonlinear behavior of this system is in fact universal[19] and can be applied to other wave-particle inter-

a)Electronic mail: matthew.lilley@chalmers.se.

actions, including those in tokamaks, by transforming to appropriate variables. The system considered in this paper consists of a purely electrostatic wave in a plasma of three species. The first two are the static background ions and "cold" electrons (characterized by mass m_e, an equilibrium density n_e, and perturbed fluid velocity V). The cold electrons respond linearly to the wave field and are subject to a small friction force providing a damping mechanism for the wave. The third is a low density population of fast electrons that are subject to "weak" (much less than the background) collisions and whose distribution function F is treated kinetically. The resulting closed system of equations is

$$\frac{\partial F}{\partial t} + v\frac{\partial F}{\partial x} - \frac{|e|E}{m_e}\frac{\partial F}{\partial v} = \left.\frac{dF}{dt}\right|_{\text{coll}}, \tag{1a}$$

$$\frac{\partial V}{\partial t} = -\frac{|e|E}{m_e} - \nu_c V, \tag{1b}$$

$$\frac{\partial E}{\partial t} = 4\pi|e|\left[n_e V + \int v(F - F_0)dv\right], \tag{1c}$$

where ν_c is the cold electron collision frequency, F_0 is the unperturbed distribution function of the fast electrons (assumed to have a constant positive slope $\partial F_0/\partial v > 0$ that determines the linear growth rate γ_L), and the right hand side of Eq. (1c) is a sum of the perturbed currents from the cold and fast electrons. The constant slope assumption is appropriate as long as the velocity range of interest is significantly narrower than the overall width of the distribution function F_0. The appropriate collision operator for the problem $(dF/dt|_{\text{coll}})$ involves three relaxation processes (diffusive, drag, and Krook-type) and is taken to be of the following form:

$$\left.\frac{dF}{dt}\right|_{\text{coll}} = D\frac{\partial^2}{\partial v^2}(F - F_0) + S\frac{\partial}{\partial v}(F - F_0) - K(F - F_0), \tag{2}$$

where D, S, and K are constants characterizing the velocity space diffusion, dynamical friction (slowing down), and Krook operators, respectively.

We investigate a traveling wave solution that has a spatial period denoted by λ and carrier frequency denoted by ω. The physical quantities can then be represented as Fourier series $F = F_0(v) + f_0(v,t) + \Sigma_{n=1}^{\infty}[f_n(v,t)\exp(in\xi) + \text{c.c.}]$, $E = 1/2 \times \Sigma_{n=1}^{\infty}[E_n(t)\exp(in\xi) + \text{c.c.}]$, and $V = \Sigma_{n=1}^{\infty}[V_n(t) \times \exp(in\xi) + \text{c.c.}]$, where $\xi \equiv kx - \omega t$ and $k \equiv 2\pi/\lambda$. Based on the previous studies, we anticipate that the physical quantities will be almost periodic in time, which means that the envelope functions f_n, E_n, and V_n vary on a time scale that is long compared to $1/\omega$. By calculating the current from the cold background perturbatively, using the assumed smallness of ν_c and $\partial[\log(V_n)]/\partial t$ with respect to ω, Ampère's law is then written as

$$\frac{\partial E_n}{\partial t}\left(1 + \frac{\omega_{pe}^2}{n^2\omega^2}\right) = in\omega\left(1 - \frac{\omega_{pe}^2}{n^2\omega^2}\right)E_n + \frac{\omega_{pe}^2}{n^2\omega^2}(-2\gamma_d)E_n + 4\pi|e|\frac{\omega}{k}\int f_n dv, \tag{3}$$

where $\gamma_d \equiv \nu_c/2$ is the damping rate of the wave. In Eq. (3) we have taken into account that the dominant contribution to the perturbed current comes from the resonant electrons with $v = \omega/k$, which allows the fast electron current to be written as

$$-|e|\int v f_n dv \approx -|e|\frac{\omega}{k}\int f_n dv. \tag{4}$$

An immediate consequence of Eq. (3) is that $\omega \approx \omega_{pe}$ when the perturbed fast electron current is small compared to that from the background population. Also $E_n \approx 0$ for $n \neq 1$ in this case so that the electric field is almost sinusoidal. Consequently, the evolution of the wave can be described by setting $\omega = \omega_{pe}$ without any loss of generality. Moreover, this formalism can describe the evolution of waves with multiple carrier frequencies as long as their frequencies do not deviate far from ω_{pe}. Then both the evolution of the amplitudes and the frequencies can be captured in the slowly varying E_1 function. This approach was previously taken for studying the spontaneous creation of holes and clumps in phase space[17] and this paper will continue this line of investigation now including the effect of dynamical friction.

As the holes and clumps evolve, the electric field becomes a sum of noninteracting BGK waves with time dependent frequencies $\omega \equiv \omega_{pe} + \delta\omega(t)$ so that the envelope $E_n(t)$ takes the form

$$E_n(t) = \sum_j \hat{E}_{n,j}(t)\exp\left[-in\int_{t_0}^{t}\delta\omega_j(t')dt'\right], \tag{5}$$

where $\hat{E}_n$ and $\delta\omega$ are real (with a proper choice of t_0). The distribution function can be written in a similar way. It is implied in Eq. (5) that $d\hat{E}_{n,j}/dt \ll \hat{E}_{n,j}\delta\omega$ and $d\delta\omega/dt \ll (\delta\omega)^2$. Ampère's law, written for each BGK mode, can then be written as

$$n\omega\left(1 - \frac{\omega_{pe}^2}{n^2\omega^2}\right)\hat{E}_{n,j} = -4\pi|e|\frac{\omega}{k}\int \text{Im}\{\hat{f}_{n,j}\}dv, \tag{6a}$$

$$\frac{\partial \hat{E}_{n,j}}{\partial t}\left(1 + \frac{\omega_{pe}^2}{n^2\omega^2}\right) = \frac{\omega_{pe}^2}{n^2\omega^2}\left(-2\gamma_d + \frac{\dot{\omega}}{\omega}\right)\hat{E}_{n,j} + 4\pi|e|\frac{\omega}{k}\int \text{Re}\{\hat{f}_{n,j}\}dv. \tag{6b}$$

Although Eqs. (6), for an individual BGK mode, are derived under the assumption that $\delta\omega \ll \omega_{pe}$, they are in fact still valid when $\delta\omega \sim \omega_{pe}$. It is not, however, the focus of this paper to explore that regime. In what follows, we limit our consideration to the case when $\delta\omega \ll \omega_{pe}$, in which case we take $\omega = \omega_{pe}$ and so the kinetic equation in the wave frame (moving with speed $v = \omega_{pe}/k$) can then be written as

$$\frac{\partial F}{\partial t} + u\frac{\partial F}{\partial \xi} - \frac{1}{2}[\omega_B^2 e^{i\xi} + \text{c.c.}]\frac{\partial F}{\partial u} = \left.\frac{dF}{dt}\right|_{\text{coll}} \tag{7}$$

and the wave equation [Eq. (3)] simplifies to

$$\frac{\partial \omega_B^2}{\partial t} - \frac{4\pi|e|^2}{m_e}\frac{\omega_{pe}}{k}\int f_1 du + \gamma_d \omega_B^2 = 0, \tag{8}$$

where $\omega_B^2 = |e|kE_1/m_e$ is the bounce frequency of the electrons trapped in the field of the wave, $u \equiv kv - \omega_{pe}$, and $\xi \equiv kx - \omega_{pe}t$. The collision operator written in the wave reference frame becomes

$$\left.\frac{dF}{dt}\right|_{\text{coll}} = \nu^3 \frac{\partial^2}{\partial u^2}(F - F_0) + \alpha^2 \frac{\partial}{\partial u}(F - F_0) - \beta(F - F_0), \tag{9}$$

where ν, α, and β are constants characterizing the velocity space diffusion, dynamical friction, and Krook operators, respectively: $\nu^3 = Dk^2$, $\alpha^2 = Sk$, and $\beta = K$. For the remainder of this paper, only drag and diffusion will be considered so that $\beta = 0$ is assumed throughout. Note that in Eq. (2) the equilibrium positive slope gives rise to a two part collision operator for drag, which is not present in the diffusion operator ($\partial^2 F_0/\partial v^2 = 0$). The $\partial F/\partial u$ term enters formally in the same way as a dc electric field. The $\partial F_0/\partial u$ part is a sink of particles that allows the formation of a steady state solution of the unperturbed distribution function (see, e.g., Ref. 20). In what follows, the first term of the drag operator will be referred to as the "dynamic part" and the second part of the drag operator will be referred to as the "sink part."

In order to explore the full nonlinearity of the system, Eqs. (7) and (8) are solved numerically using a scheme similar to Ref. 17. More specifically, the Fourier series representation of F in space transforms Eq. (7) into a set of coupled partial differential equations in t and u. By Fourier transforming in velocity, a set of advection equations is then obtained for numerical processing using the BOT code (see the Appendix). The key advantages of BOT are high speed, the simplicity of collisions in Fourier space (they are represented algebraically), and the convenient procedure for eliminating small scales in velocity space.

Unless otherwise stated, a fixed damping rate $\gamma_d/\gamma_L = 0.9$ will be used for the BOT simulations, which is close enough to the threshold to be considered marginal. This is the regime in which holes and clumps were previously observed to form spontaneously. When BOT results are displayed in subsequent figures, the simulation parameters are either the defaults given in the Appendix or they are displayed above the figure (see Appendix for notation).

III. BENCHMARKING

In the collisionless, dissipationless limit ($\nu = \alpha = \gamma_d = 0$), the system is predicted to saturate with an electric field corresponding to a bounce frequency of $\omega_B/\gamma_L \approx 3.2$.[21] The saturated distribution function is then predicted to form a plateau inside a region of phase space defined by the wave separatrix. In this case, the particles that are trapped by the wave potential (those inside the wave separatrix) become "phase-mixed" over time. In this way, the distribution function remains a monotonic function of velocity with a narrow flat region around the resonance. The BOT code reproduces the saturation and phase mixing with good accuracy, as can be seen in Figs. 1 and 2.

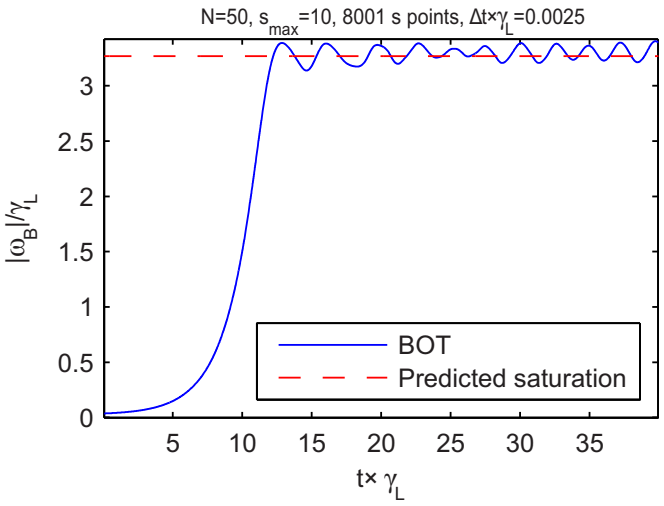

FIG. 1. (Color online) Collisionless, dissipationless saturation. The solid line shows the bounce frequency for the BOT simulation and the dashed line shows the predicted saturation level (Ref. 21).

In the presence of diffusive collisions only ($\alpha = 0$), the nonlinear amplitude evolution of a wave excited close to the threshold ($\gamma_d \approx \gamma_L$) is predicted to exhibit four main regimes, in order of decreasing ratio of $\nu/(\gamma_L - \gamma_d)$:[19] (1) a steady state regime, (2) a regime with periodic amplitude modulation, (3) a chaotic regime, and (4) an "explosive" regime. All regimes are recovered with the BOT code, noting that the explosive regime leads to the spontaneous formation of holes and clumps in phase space, which is discussed in more detail in Sec. IV. Figure 3 shows a case of mode saturation. The results from the BOT simulation and the "cubic equation" [Eq. 14 in Ref. 19] converge as the threshold is approached, as expected, noting that the intermediate dynamics also converge along with the saturation level. Figure 4 shows an

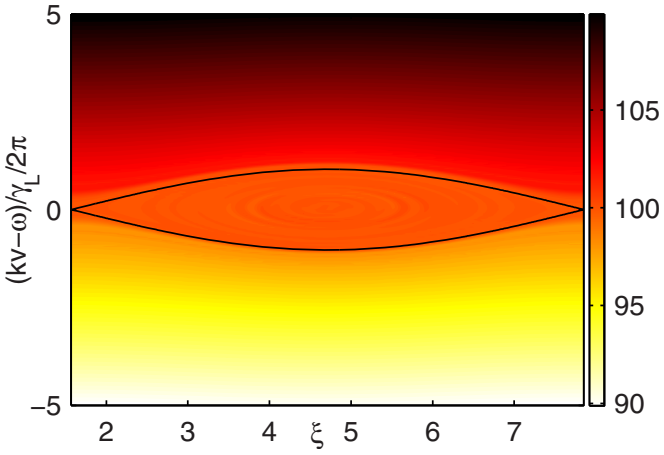

FIG. 2. (Color online) Phase space plot showing contours of F corresponding to Fig. 1 at $t \times \gamma_L = 40$. The black line corresponds to the wave separatrix. A contour equal to 100 corresponds to the level of the original resonance.

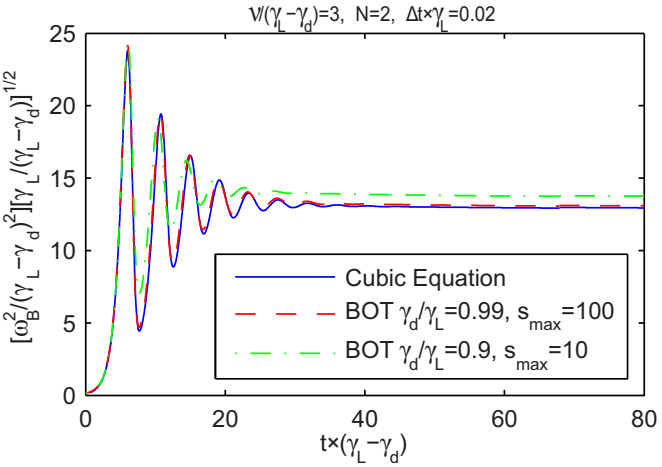

FIG. 3. (Color online) Comparison of the BOT simulation with the cubic equation (Ref. 19) in the marginally unstable regime with pure diffusion. The bounce frequency is normalized according to Ref. 18.

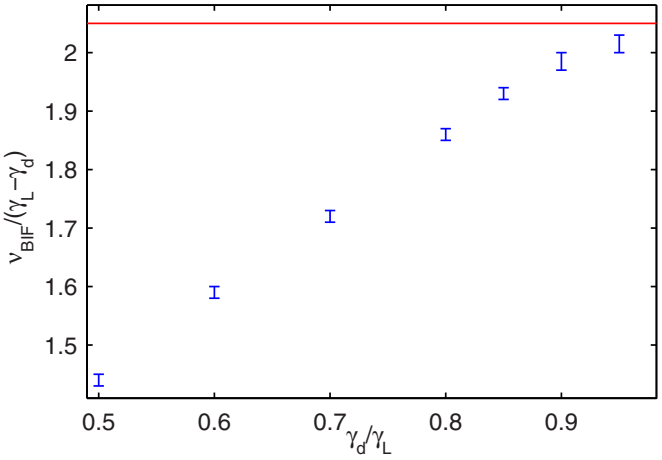

FIG. 5. (Color online) Numerically observed bifurcation is seen to occur between the error bars for a given dissipation rate, with pure diffusion. The results were obtained in the same way as those in Fig. 4. The analytical bifurcation threshold value of 2.05 is shown by the solid line (Ref. 19).

example of the transition from the saturated to the periodic amplitude modulated case. Note that this transition (called the first bifurcation) is marked by a critical diffusion coefficient of $\nu_{\mathrm{BIF}}/(\gamma_L-\gamma_d)\approx 2.05$.[19] This coefficient is also recovered by the BOT simulations to within 2.5% as the threshold is approached, as can be seen in Fig. 5. Finally, Fig. 6 shows an example of the chaotic regime.

In the presence of drag and diffusive collisions, the predicted nonlinear amplitude evolution is governed by Eq. 4 of Ref. 16. The BOT simulations agree to the same accuracy as in the pure diffusive case.

IV. HOLES AND CLUMPS

A. Collisionless limit

The strongly nonlinear "hole-clump" scenario described in Ref. 14 is observed in the marginally unstable regime, as can be seen from the spectrogram in Fig. 7 and in the phase space plot in Fig. 8. The holes and clumps move away from the original resonance, as shown schematically in Fig. 9. This motion is almost adiabatic and preserves the value of the distribution function for the particles trapped by the wave.

We note that within this simplified theory there is no limit to the extent of the chirp, and this is indeed supported by the simulation. The chirping behavior shows the correct $\sqrt{t}$ scaling, noting that the associated coefficient is larger than predicted analytically[14] by a factor of approximately 1.32 in this case. This discrepancy could result from the nonuniformity of the distribution function along the wave separatrix that is seen in Fig. 8, this is not included in the analytical theory. How the system sustains this nonuniform distribution will be the focus of future investigation.

It may look surprising that holes (seen as upward sweeping spectral lines in Fig. 7) and clumps (seen as downward sweeping spectral lines in Fig. 7) are generated continuously in the collisionless case, without any source of particles. This can be understood by following the evolution of the "wake"

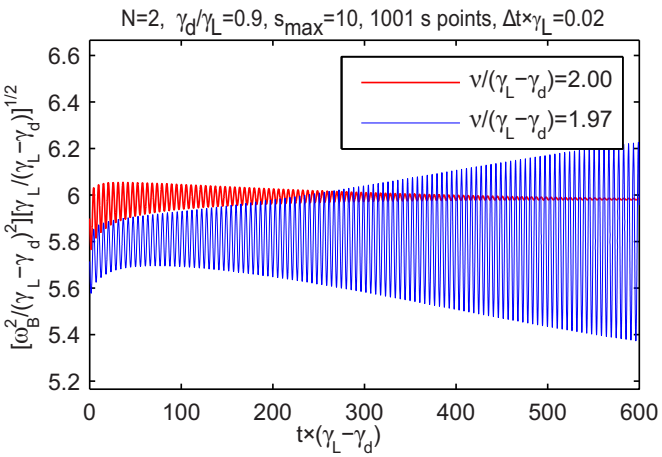

FIG. 4. (Color online) Transition from steady state saturation (thick line) to a limit cycle (thin line) in the marginally unstable regime with pure diffusion. The bounce frequency is normalized according to Ref. 18. These results were obtained by initializing the BOT code deep in the saturated region, $\nu/(\gamma_L-\gamma_d)=3$. The diffusive collision frequency was then reduced over time to the levels in the figure. The resulting electric field and distribution function were then used as initial conditions in the BOT code. In this way, one avoids the very long transient behavior that obscures the periodic modulation.

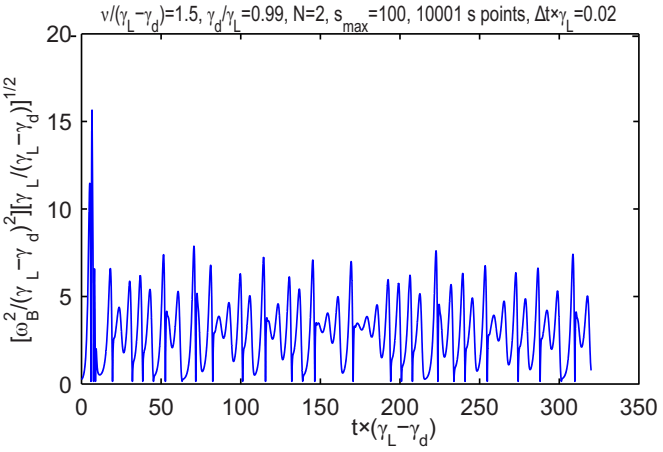

FIG. 6. (Color online) The chaotic regime in the marginally unstable case with pure diffusion. The bounce frequency normalized according to Ref. 18.

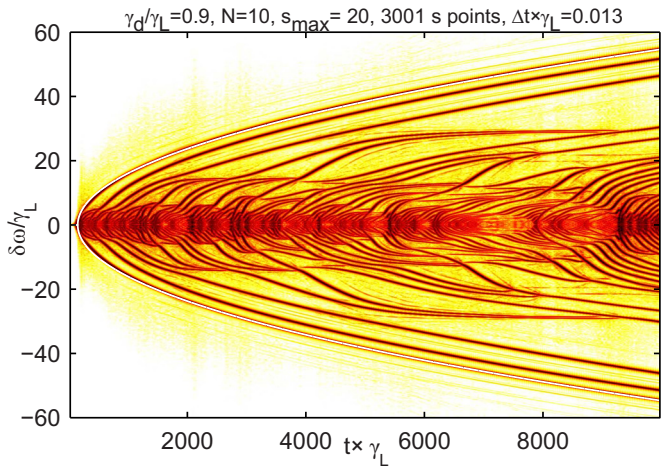

FIG. 7. (Color online) Spectrogram of the electric field amplitude E_1 for the collisionless case close to the threshold. The white line is the best $\sqrt{t}$ fit passing through the upper and lower chirping structures.

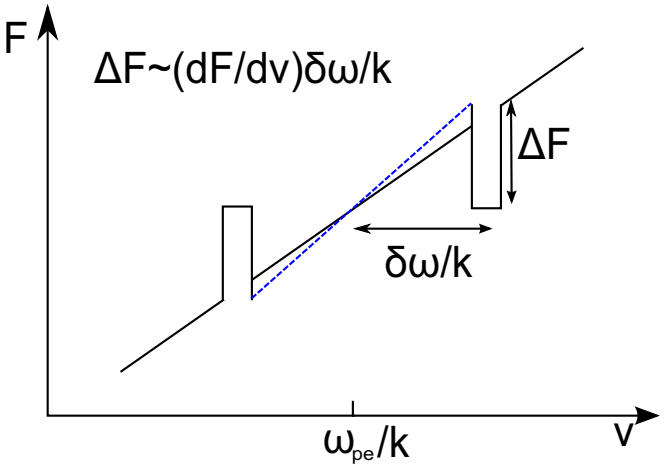

FIG. 9. (Color online) Cartoon illustrating the motion of holes and clumps and the wake (dotted line) that acts to steepen the distribution function, creating a favorable environment for instability.

that forms when a hole or a clump detaches from the original resonance. Referring to Fig. 9, since the particle number is conserved, a number of particles must be displaced during the motion of a hole or a clump, which leads to a slight excess behind a hole and a depletion behind a clump. There is thus a tendency for the gradient in the distribution function to steepen, making the system susceptible to instability once again. This effect should be strongest when the hole and clump are still relatively close to the original resonance, which could explain why the holes and clumps are produced in rapid succession. In reality the finite extent of the distribution in velocity space limits the range of chirping for the initially formed holes and clumps. It is then reasonable to expect that eventually the holes and clumps will "stack up" next to one another as they move away from the original resonance (see Fig. 10). In this way, the distribution function should eventually form a global plateau that determines the maximum amount of energy that can be released from the fast particles to the wave. At this point, the wave should then decay due to dissipation, leaving behind a significantly deformed fast electron distribution.

B. The effect of drag

The drag introduces a preferred direction of particle flow into the system. Consequently, one can expect the symmetry observed in Fig. 7 to be broken when drag is introduced and this is indeed found to be the case [Fig. 11(a)].

To understand the results shown in Fig. 11, we consider the effect of drag on a single hole or clump, the formal description of which is given by Eqs. (6a) and (6b). First we calculate the power transfer from the particles to the wave in the presence of drag in the adiabatic regime ($\alpha \ll \omega_B$). The drag operator consists of a dynamic part and a sink for the particles. The former acts as a constant force slowing the particles down, and the latter acts to lower the distribution function. The wave separatrix determines an area of phase

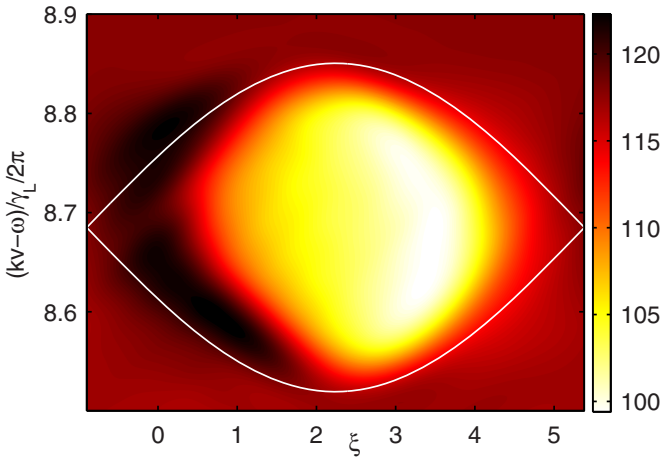

FIG. 8. (Color online) Phase space plot showing contours of F for the hole corresponding to the highest frequency in Fig. 7 at $t \times \gamma_L = 10\,000$. The white line marks the wave separatrix for the hole with $\omega_B/\gamma_L \approx 0.5$. A contour equal to 100 corresponds to the level of the original resonance.

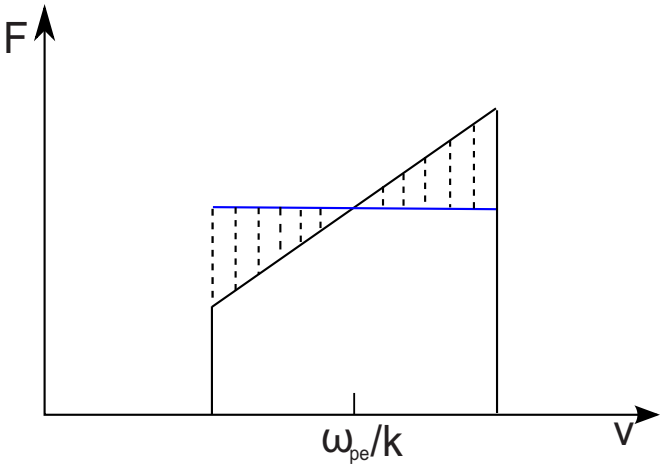

FIG. 10. (Color online) Cartoon illustrating how holes and clumps might form a global plateau in a distribution function with a finite extent in velocity space. The dashed lines mark the boundaries of the "stacked up" holes and clumps.

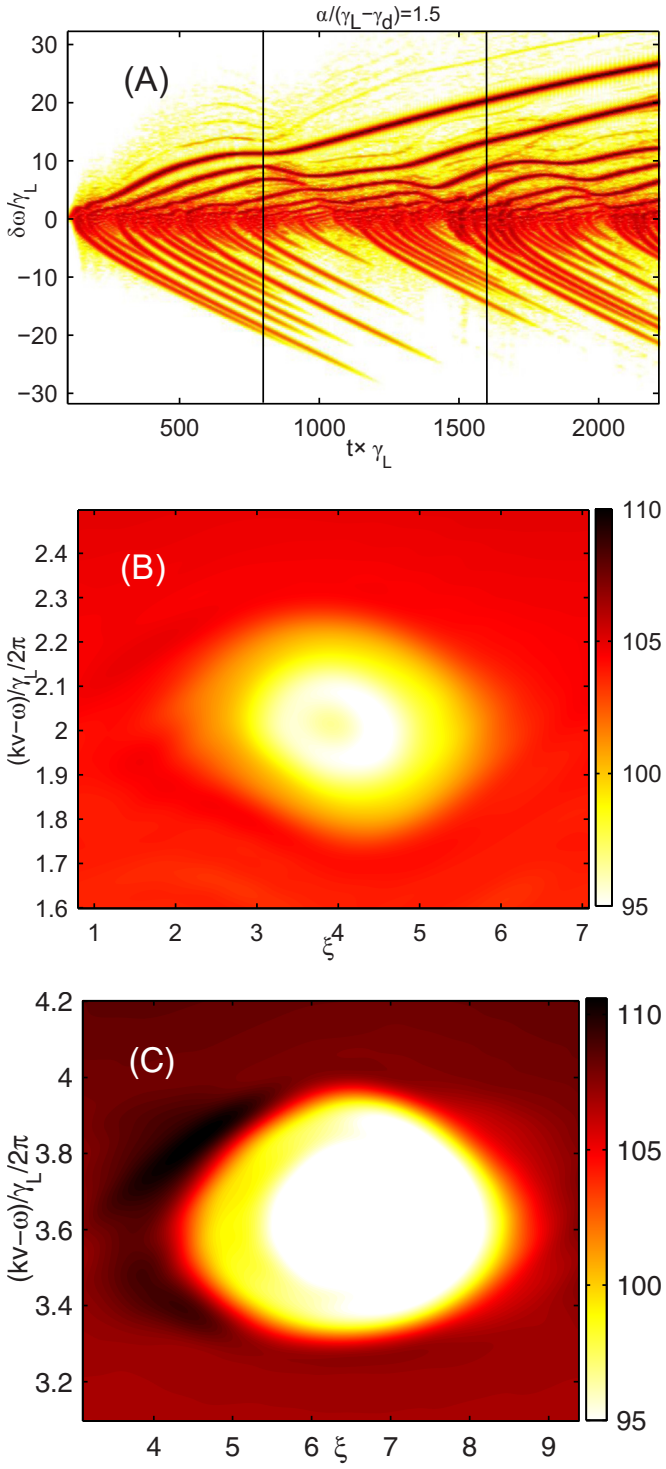

FIG. 11. (Color online) (a) Spectrogram of the electric field amplitude E_1 showing chirping asymmetry for the pure drag case. [(b) and (c)] Snap shots (at $t\times\gamma_L=800$ and $t\times\gamma_L=1600$) of the phase space for the upper most spectral line showing a deepening hole. A contour equal to 100 corresponds to the level of the original resonance.

space filled with trapped particles and its location in velocity space is given by the phase velocity of the wave ω/k. The dynamic part of the drag operator creates a flow of passing particles toward the separatrix at a rate of α^2/k. However, the particles that approach the separatrix are unable to enter and instead they make a "jump" to a velocity that is lower by an amount given by the separatrix width $\Delta v(\xi)$. The corresponding energy release can be calculated using the same line of reasoning as that in Refs. 14 and 22. When considering the flow over the entire separatrix (from $0<\xi<2\pi$), the power released to the wave per unit volume is given by

$$\delta\epsilon^{+}_{\mathrm{drag}} = f_{\mathrm{out}}\frac{\alpha^2}{k}\times m_e\frac{\omega_{pe}}{k}\int_0^{2\pi}\Delta v d\xi, \tag{10}$$

where the separatrix width $\Delta v(\xi)$ is assumed to be small compared to the wave phase velocity, which is close to ω_{pe}/k, and f_{out} is the value of the distribution function just outside the separatrix. For the trapped particles, moving with an approximate speed ω_{pe}/k, the electric field works against the drag force ($m_e\alpha^2/k$ per particle) to keep them inside the separatrix. The separatrix acts as a rigid boundary for the particles in the adiabatic regime. Note that the work done is insensitive to the details of the distribution inside the separatrix, it only depends on the total number of trapped particles. The rate of work done by the electric field on the trapped particles must balance the work done against the drag force, which, per unit volume, is approximately given by

$$\delta\epsilon^{-}_{\mathrm{drag}} = f_{\mathrm{in}}\int_0^{2\pi}\Delta v d\xi\times m_e\frac{\alpha^2}{k}\frac{\omega_{pe}}{k}, \tag{11}$$

where the distribution function f_{in} is assumed to be constant inside the separatrix. The net power released as a result of this dynamic part is then given by

$$\delta\epsilon_{\mathrm{drag}} = [f_{\mathrm{out}}-f_{\mathrm{in}}]\int_0^{2\pi}\Delta v d\xi m_e\frac{\alpha^2}{k}\frac{\omega_{pe}}{k}. \tag{12}$$

Hence, for a hole drag will channel energy to the wave and for a clump energy will be taken. If the phase velocity and hence the frequency of the wave changes, there will be a similar release of energy if a hole moves up or a clump moves down in phase space, and this energy release is proportional to the rate of chirping and the difference in height of the ambient distribution function and that within the separatrix,[14,22]

$$\delta\epsilon_{\mathrm{chirp}} = [f_{\mathrm{out}}-f_{\mathrm{in}}]\int_0^{2\pi}\Delta v d\xi m_e\frac{1}{k}\frac{\partial\delta\omega}{\partial t}\frac{\omega_{pe}}{k}. \tag{13}$$

If the amplitude of the wave is changing slowly, $\partial[\log(\hat{E}_1)]/\partial t\ll\gamma_d$, then an energy balance condition can be constructed so that the energy dissipated by the background plasma, $\gamma_d|\hat{E}_1|^2/4\pi$, is balanced by the work done by the electric field on the fast particles, $\delta\epsilon_{\mathrm{drag}}+\delta\epsilon_{\mathrm{chirp}}$. Note that the integrals in Eqs. (12) and (13) can be estimated as ω_B/k. At this point, it is convenient to introduce a function g that characterizes the depth of a hole $[f_{\mathrm{out}}-f_{\mathrm{in}}]=(\partial F_0/\partial v)g/k\sim\gamma_L g k n_e/\omega_{pe}^3$ in a way similar to that shown in Fig. 9. The energy balance condition can then be written as

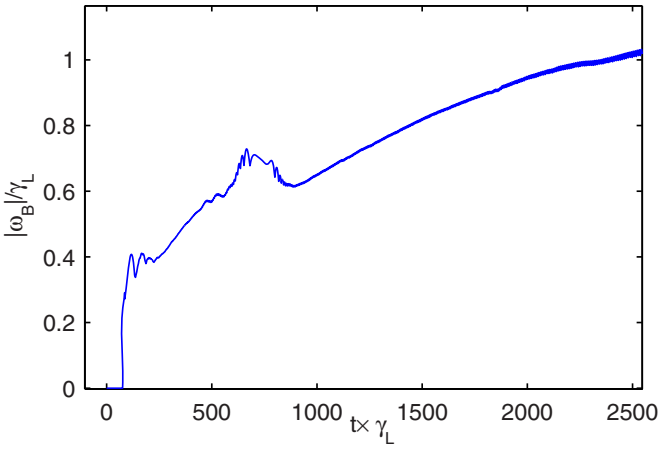

FIG. 12. (Color online) Drag induced growth of the bounce frequency corresponding to the upper most spectral line in Fig. 11(a).

$$(c_1\omega_B)^3 = g\left(\frac{\partial\delta\omega}{\partial t} + \alpha^2\right), \tag{14}$$

when $\gamma_L \approx \gamma_d$ and where c_1 is a constant. Note that presence of drag in this energy balance allows a downward motion of a hole structure, something that was previously forbidden. This equation, which is equivalent to Eq. (6b), involves three unknown functions: ω_B, $\delta\omega$, and g. We now derive two more equations for these unknowns to obtain a complete set.

The effect of the sink part of the drag operator is to reduce the height of a clump and to deepen a hole linearly with time. In this way, the drag is acting to destroy a clump structure but to enhance a hole. As a result of drag and chirping, the depth/height evolves in time according to

$$\frac{\partial g}{\partial t} = \frac{\partial\delta\omega}{\partial t} + \alpha^2. \tag{15}$$

The final relation follows from Eq. (6a) with $n=1$ and $\delta\omega \ll \omega_{pe}$. We note that the dominant contribution to the perturbed charge density of the fast electrons comes from the narrow depletion (hole) or protrusion (clump) in the distribution function so that Eq. (6a) gives the following estimate:

$$\delta\omega c_1\omega_B = c_2\gamma_L g, \tag{16}$$

where c_2 is a constant. When considering the long time evolution of a drag dominated hole, one can neglect $\partial\delta\omega/\partial t$ as compared to α^2 in Eqs. (14) and (15) to find the following scaling:

$$\omega_B \sim \alpha^{4/3}t^{1/3}, \quad \delta\omega \sim \gamma_L(\alpha t)^{2/3} \tag{17}$$

for an upward chirping hole. The immediate consequence is that the hole cannot reach a steady state. The frequency and amplitude of the wave will increase continuously, as can be seen in Figs. 11(a) and 12. The depth of the hole also increases, which is consistent with Figs. 11(b) and 11(c).

In the absence of the drag sink term $(\partial F_0/\partial u)$, the depth of the hole is $g=\delta\omega$ and a steady state is permitted. This can be demonstrated numerically by removing the slope of the equilibrium distribution after the initial instability has been seeded. The results are shown in Fig. 13 where the slope is removed at a time $t\times\gamma_L=800$.

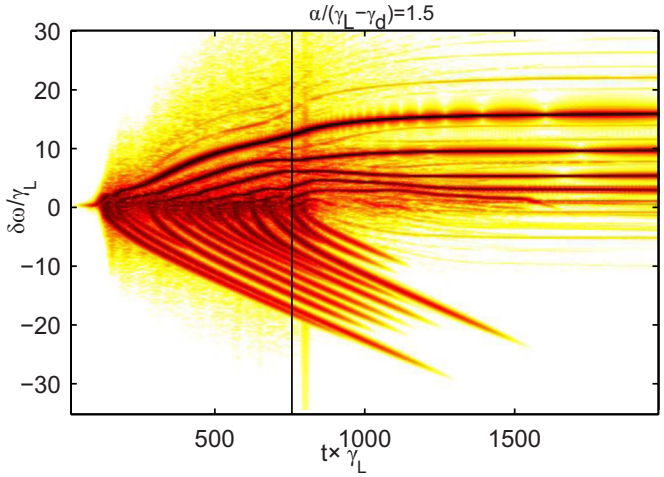

FIG. 13. (Color online) Establishment of steady state holes by the removal of the drag sink at $t\times\gamma_L=800$.

We conclude this section by recalling that dynamical friction was found to be destabilizing in the weak nonlinear approximation studied in Ref. 16. Now in the fully nonlinear regime, dynamical friction continues to provide a destabilizing effect.

C. Drag and diffusion

In reality, a system will exhibit both drag and diffusion. The effect of diffusion, unlike drag, is always to act to destroy a hole and a clump by filling the hole and depleting the clump. For a phase space structure whose characteristic size in velocity space is approximately $\Delta v=\Delta\Omega/k$, the decay time as a result of diffusion is approximately $\tau_D \sim \Delta\Omega^2/\nu^3$. We observe that a steady hole can be established when both drag and diffusion are present, as can be seen in Fig. 14.

With somewhat more diffusion, there is a tendency for the frequency and the electric field to undulate (Fig. 15). With a further increase in diffusion, the frequency spectrum

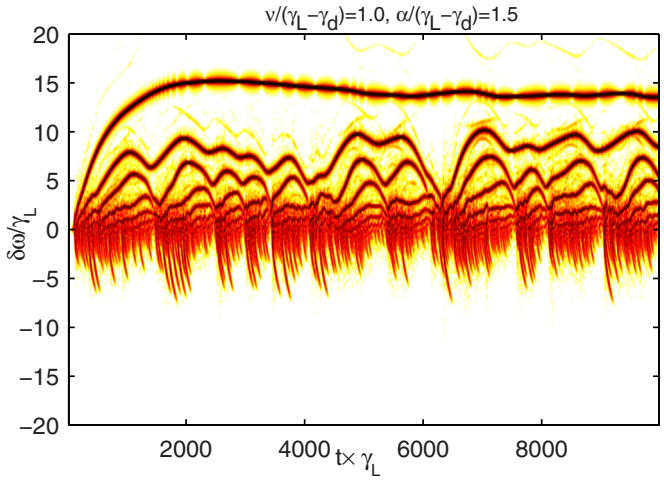

FIG. 14. (Color online) Establishment of a steady state hole in the presence of both drag and diffusion.

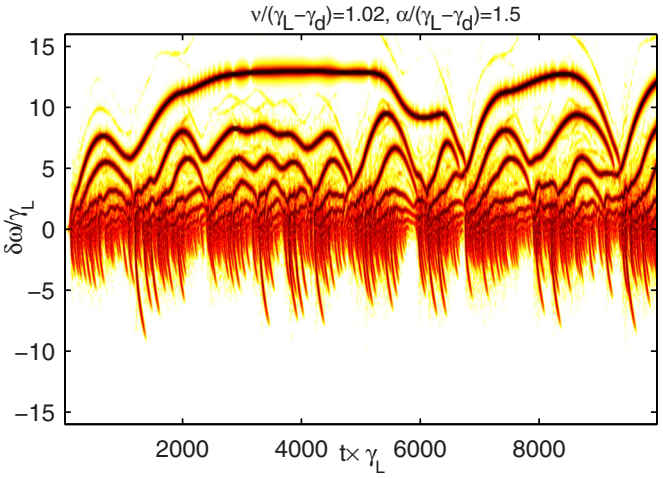

FIG. 15. (Color online) Undulating frequency and amplitude behavior with drag and somewhat more diffusion than in Fig. 14.

exhibits intermittent hooks (Fig. 16). It is noteworthy that these hooks resemble experimentally observed chirping patterns.[23]

These behaviors can be understood by recognizing the competition that now exists between the sink in the drag collision operator that acts to deepen the hole and the diffusion that acts to fill the hole. This competition can be modeled using Eqs. (14)–(16), with Eq. (15) modified to account for the effect of diffusion on the depth of the hole. The resulting set of dynamical equations is then

$$(c_1\omega_B)^3 = g\left(\frac{\partial \delta\omega}{\partial t} + \alpha^2\right), \tag{18a}$$

$$\frac{\partial g}{\partial t} + \frac{\nu^3}{c_3(c_1\omega_B)^2}g = \frac{\partial \delta\omega}{\partial t} + \alpha^2, \tag{18b}$$

$$\delta\omega c_1\omega_B = c_2\gamma_L g, \tag{18c}$$

where c_3 is a free parameter of order unity. These equations reduce to

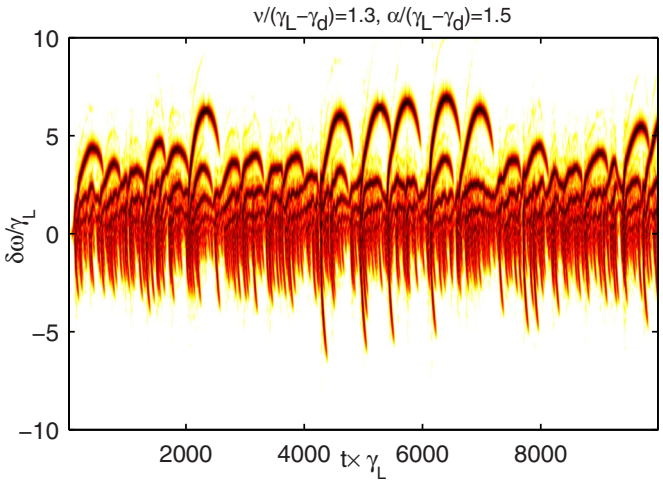

FIG. 16. (Color online) Hooked frequency spectrum with drag and a further increase in diffusion from that in Fig. 15.

$$x^2 = y\left(\frac{\partial y}{\partial \tau} + 1\right), \tag{19a}$$

$$a\frac{\partial(xy)}{\partial \tau} + \frac{y}{x} = \left(1 + \frac{\partial y}{\partial \tau}\right), \tag{19b}$$

where $c_1\omega_B \equiv c_3\alpha^4 x/\nu^3$, $\delta\omega \equiv \alpha^6 c_2 c_3^2 \gamma_L y/\nu^6$, $t \equiv \alpha^4 c_2 c_3^2 \gamma_L \tau/\nu^6$, and $a \equiv c_3\alpha^4/\nu^3 c_2\gamma_L$. Equations (19) exhibit a steady state at $x=1$, $y=1$. By analyzing the stability of this solution, we find small deviations from the steady state evolve as $\exp(\lambda\tau)$ with the following eigenvalues:

$$\lambda = \frac{-3(a-1) \pm \sqrt{9(a-1)^2 - 4a}}{2a}. \tag{20}$$

Thus, the steady state is stable for $a>1$ and unstable for $a<1$.

In order to compare this simple model to the results from the BOT simulations, the coefficients c_1, c_2, and c_3 must be chosen. c_1 and c_2 are determined by comparing the solution of Eqs. (18) at early times (when $g=\delta\omega$ and collisions can be neglected) with the following expressions for ω_B and $\delta\omega$ given in Ref. 14:

$$\frac{\delta\omega}{\gamma_L} = \frac{16\sqrt{2}}{3\pi^2\sqrt{3}}\sqrt{\gamma_d t}, \tag{21a}$$

$$\frac{\omega_B}{\gamma_L} = \frac{16}{3\pi^2}. \tag{21b}$$

This gives $c_1=(3\pi^2/48)^{1/3}$ and $c_2/c_1=16/3\pi^2$. The value of c_3 is determined by comparing the stability condition $a \equiv c_3\alpha^4/\nu^3 c_2\gamma_L=1$ from Eqs. (19) with the stability boundary obtained numerically for the case $\nu=\alpha$. This gives $c_3=1.84$.

Figure 14 can now be related to the stable solution of Eqs. (19) since $a=2.02$ in this case. More specifically, the asymptotic value of $\delta\omega$ is calculated to be $\delta\omega/\gamma_L \approx 17.7$, and the relaxation time, defined to be $\tau=1/\mathrm{Re}\,\lambda$, gives $t\times\gamma_L \approx 1600$. This agrees well with the simulation.

Figure 16 represents the unstable case with $a=0.92$. A numerical solution of Eqs. (19) [shown in Fig. 17(a)] reproduces the evolution of a single hook. The frequency and time scales are in good quantitative agreement with the well isolated hooks seen in Fig. 16, as shown in Fig. 17(b). For Fig. 15, $a=1.91$. Based on this value, one would expect that a single hole should evolve to a steady state. However, the correlation seen between different spectral lines in Fig. 15 suggests that there is some hole-hole interaction (not covered in this model) that produces the undulating behavior.

V. SUMMARY

The destabilizing effect of drag, which was predicted in Ref. 16, has now been shown to continue to be destabilizing in the fully nonlinear regime. The clear signature of drag is the asymmetry of the wave evolution with respect to the original resonance. Drag provides an energy source for the wave in a way similar to chirping. The source term in the drag collision operator acts to enhance a phase space hole

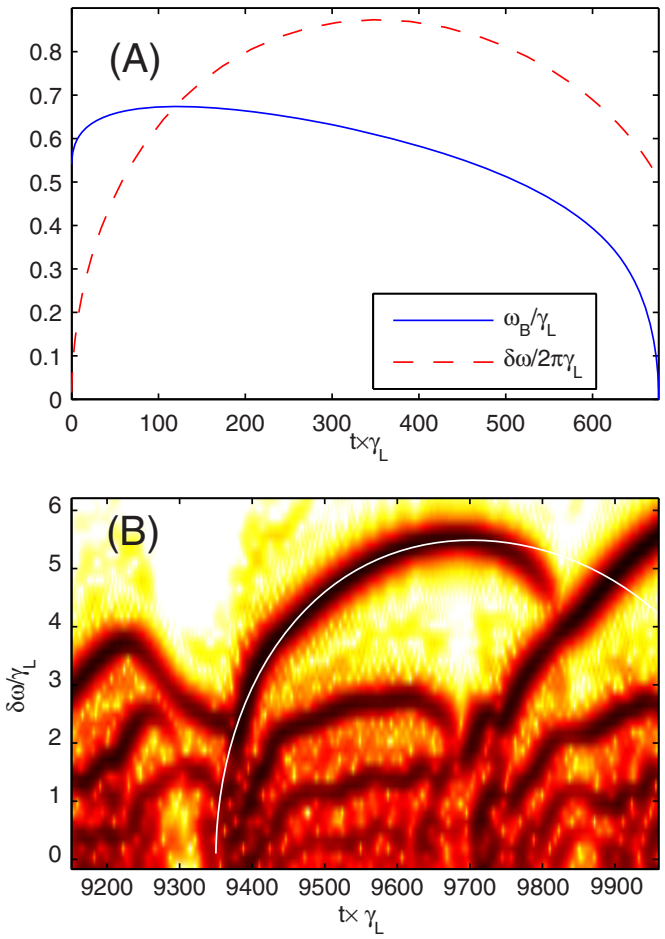

FIG. 17. (Color online) (a) Hooked chirp solution of Eqs. (19) with $c_1^3=3\pi^2/48$, $c_2/c_1=16/3\pi^2$, $c_3=1.84$, $\alpha/\gamma_L=0.15$, and $\nu/\gamma_L=0.13$; the solid and dashed lines show the bounce frequency and the deviation of the frequency from the plasma frequency, respectively. (b) A quantitative agreement between hooks seen in Figs. 16 and 17(a) (white line) is shown.

and to weaken, or even suppress, a phase space clump. The combined effect of drag and velocity space diffusion allows a steady state hole to be established. It can also produce a repetitive pattern of hooked frequency chirping. These behaviors have been captured by a reduced analytical model. The full scale simulations agree with the trends of this model. The resemblance between the hooked chirping pattern and that seen in experiments is an interesting topic for further investigation. Another natural next step would be to extend the presented results, on the basis of Eqs. (6), to the case when the range of frequency sweeping is comparable to the plasma frequency.

ACKNOWLEDGMENTS

The authors are grateful to M. Lisak for his interest in this work and for his support that made this collaboration possible. This work was funded jointly by the Swedish Research Council, the UK EPSRC-GB Grant No. EP/G003955, the EURATOM, and the U.S Department of Energy Contract No. DE-FG03-96ER-54326.

APPENDIX: BOT EQUATIONS

Referring to Eqs. (7) and (8), we define $C=\omega_B^2/\gamma_L^2$, where $\omega_B^2=|e|kE_1/m$, $G=(2\pi|e|^2\omega_{pe}/m\gamma_L^2k)F$, $\tau=\gamma_L t$, $\hat{\gamma}_d=\gamma_d/\gamma_L$, $\Omega=(kv-\omega_{pe})/\gamma_L$, $\bar{\nu}=\nu/\gamma_L$, and similarly for $\bar{\alpha}$ and $\bar{\beta}$. Using these variables and Fourier transforming Eq. (7) in Ω gives

$$\frac{\partial \mathcal{G}_n}{\partial \tau}-n\frac{\partial \mathcal{G}_n}{\partial s}+[\bar{\nu}^3s^2-i\bar{\alpha}^2s+\bar{\beta}]\mathcal{G}_n=R_n(s,\tau), \tag{A1}$$

$$\frac{\partial C}{\partial \tau}+\hat{\gamma}_d C=2\sqrt{2\pi}\mathcal{G}_1(0,\tau), \tag{A2}$$

where $\mathcal{G}_n=(1/\sqrt{2\pi})\int_{-\infty}^{+\infty}G_n\exp(-i\Omega s)d\Omega$ is the Fourier transform of G_n and $R_n(s,\tau)$ is given by

$$R_0=\frac{is}{2}[C^*\mathcal{G}_1(s,\tau)+C\mathcal{G}_1^*(-s,\tau)], \tag{A3a}$$

$$R_1=\frac{is}{2}[C^*\mathcal{G}_2(s,\tau)+C\mathcal{G}_0(s,\tau)]+\frac{1}{\sqrt{2\pi}}C\delta(s), \tag{A3b}$$

$$R_n=\frac{is}{2}[C^*\mathcal{G}_{n+1}(s,\tau)+C\mathcal{G}_{n-1}(s,\tau)], \tag{A3c}$$

$$R_N=\frac{is}{2}[C\mathcal{G}_{N-1}(s,\tau)], \tag{A3d}$$

and where the number of harmonics of F, N, is determined by numerical convergence. Similar equations can be also cast for the case when the wave electric field has several spatial harmonics, and the BOT code includes this capability; however, for simplicity, only the single harmonic sinusoidal case is shown in this paper.

The kinetic equation now forms a set of coupled advection equations in s with an algebraic collision operator. Structures in F "flow" to larger $|s|$ and hence to smaller scales in velocity space. The smallest scales do not contribute to the current that drives the electric field, so they are eliminated by choosing an appropriate box size in s. In the presence of diffusion, the box size is chosen so that $|s|_{\max}\sim 1/\bar{\nu}$. Without diffusion the box size is varied until convergence is achieved. The kinetic equation is integrated in time by the method of characteristics (i.e., transforming to $s'=s+n\tau$, $\tau'=\tau$). This produces a set of integral equations that are not subject to the Courant limit that would arise from using a standard finite difference technique. The trapezoid rule is then used to calculate the time integrals. The contribution from the equilibrium distribution [which is the delta function in Eq. (A3b)] is integrated analytically. The time step $\Delta\tau$ is set to be an integer multiple of Δs so that the advection procedure is performed perfectly, without the need to interpolate the distribution function. This is advantageous since the contribution from the delta function to $\mathcal{G}_1$ creates a discontinuity in $\mathcal{G}_n$ that is not easily captured by interpolation. A default simulation with 1001 points in s, a box with $|s|_{\max}=10$, $N=10$, $\Delta\tau=0.02$, $\Delta\tau=\Delta s$, $\gamma_d/\gamma_L=0.9$, and a run time of $\tau_{\max}=5000$, takes about 10 min on a single dual core Intel Centrino processor.

[1]A. Fasoli, C. Gormenzano, H. L. Berk, B. N. Breizman, S. Briguglio, D. S. Darrow, N. N. Gorelenkov, W. W. Heidbrink, A. Jaun, S. V. Konovalov, R. Nazikian, J.-M. Noterdaeme, S. E. Sharapov, K. Shinohara, D. Testa, K. Tobita, Y. Todo, G. Vlad, and F. Zonca, Nucl. Fusion **47**, S264 (2007).
[2]S. E. Sharapov, B. Alper, J. Fessey, N. C. Hawkes, N. P. Young, R. Nazikian, G. J. Kramer, D. N. Borba, S. Hacquin, E. De La Luna, S. D. Pinches, J. Rapp, D. Testa, and JET-EFDA Contributors, Phys. Rev. Lett. **93**, 165001 (2004).
[3]A. Fasoli, B. N. Breizman, D. Borba, R. F. Heeter, M. S. Pekker, and S. E. Sharapov, Phys. Rev. Lett. **81**, 5564 (1998).
[4]R. F. Heeter, A. F. Fasoli, and S. E. Sharapov, Phys. Rev. Lett. **85**, 3177 (2000).
[5]K. L. Wong, J. R. Wilson, Z. Y. Chang, G. Y. Fu, E. Fredrickson, G. W. Hammett, C. Bush, C. K. Phillips, J. Snipes, and G. Taylor, Plasma Phys. Controlled Fusion **36**, 879 (1994).
[6]M. Saigusa, H. Kimura, S. Moriyama, Y. Neyatani, T. Fujii, Y. Koide, T. Kondoh, M. Sato, M. Nemoto, and Y. Kamada, Plasma Phys. Controlled Fusion **37**, 295 (1995).
[7]S. Bernabei, R. V. Budny, E. D. Fredrickson, N. N. Gorelenkov, J. C. Hosea, C. K. Phillips, R. B. White, J. R. Wilson, C. C. Petty, R. I. Pinsker, R. W. Harvey, and A. P. Smirnov, Nucl. Fusion **41**, 513 (2001).
[8]J. A. Snipes, N. Basse, C. Boswell, E. Edlund, A. Fasoli, N. N. Gorelenkov, R. S. Granetz, L. Lin, Y. Lin, R. Parker, M. Porkolab, J. Sears, S. E. Sharapov, V. Tang, and S. Wukitch, Phys. Plasmas **12**, 056102 (2005).
[9]S. D. Pinches, H. L. Berk, M. P. Gryaznevich, S. E. Sharapov, and JET-EFDA Contributors, Plasma Phys. Controlled Fusion **46**, S47 (2004).
[10]E. Fredrickson, N. Gorelenkov, R. Bell, J. Menard, A. Roquemore, S. Kubota, N. Crocker, and W. Peebles, Nucl. Fusion **46**, S926 (2006).
[11]K. L. Wong, R. J. Fonck, S. F. Paul, D. R. Roberts, E. D. Fredrickson, R. Nazikian, H. K. Park, M. Bell, N. L. Bretz, R. Budny, S. Cohen, G. W. Hammett, F. C. Jobes, D. M. Meade, S. S. Medley, D. Mueller, Y. Nagayama, D. K. Owens, and E. J. Synakowski, Phys. Rev. Lett. **66**, 1874 (1991).
[12]W. Heidbrink, E. Strait, E. Doyle, G. Sager, and R. Snider, Nucl. Fusion **31**, 1635 (1991).
[13]K. Shinohara, Y. Kusama, M. Takechi, A. Morioka, M. Ishikawa, N. Oyama, K. Tobita, T. Ozeki, S. Takeji, S. Moriyama, T. Fujita, T. Oikawa, T. Suzuki, T. Nishitani, T. Kondoh, S. Lee, M. Kuriyama, JT-60 Team, G. J. Kramer, N. N. Gorelenkov, R. Nazikian, C. Z. Cheng, G. Y. Fu, and A. Fukuyama, Nucl. Fusion **41**, 603 (2001).
[14]H. L. Berk, B. N. Breizman, and N. V. Petviashvili, Phys. Lett. A **234**, 213 (1997).
[15]I. B. Bernstein, J. M. Greene, and M. D. Kruskal, Phys. Rev. **108**, 546 (1957).
[16]M. K. Lilley, B. N. Breizman, and S. E. Sharapov, Phys. Rev. Lett. **102**, 195003 (2009).
[17]N. Petviachvili, Ph.D. thesis, University of Texas at Austin, 1999.
[18]H. L. Berk, B. N. Breizman, and M. Pekker, Phys. Rev. Lett. **76**, 1256 (1996).
[19]B. N. Breizman, H. L. Berk, M. S. Pekker, F. Porcelli, G. V. Stupakov, and K. L. Wong, Phys. Plasmas **4**, 1559 (1997).
[20]H. L. Berk and B. N. Breizman, Phys. Fluids B **2**, 2226 (1990).
[21]See National Technical Information Service Document No. AD730123 PGG-93 (B. Fried, C. Lui, W. Means, and R. Sagdeev, University of California Report No. AD730123 PGG-93, 1971). Copies may be ordered from the National Technical Information Service, Springfield, Virginia 22161.
[22]B. N. Breizman, Nucl. Fusion **50**, 084014 (2010).
[23]H. Berk, C. Boswell, D. Borba, A. Figueiredo, T. Johnson, M. Nave, S. Pinches, S. Sharapov, and JET-EFDA Contributors, Nucl. Fusion **46**, S888 (2006).